Resonant resistive instability of a high-current relativistic electron beam in plasma

L. E. Aranchuk, V. D. Vikharev, V. V. Gorev, S. F. Zhandarov, S. V. Zakharov, V. D. Korolev, V. P. Smirnov, and L. I. Urutskoev

I. V. Kurchatov Institute of Atomic Energy

(Submitted 28 August 1983)
Zh. Eksp. Teor. Fiz. **86**, 1280–1295 (April 1984)

The instability of a relativistic electron beam in finite-conductivity plasma produced by injecting the beam into a gas is investigated. The instability arises as a result of the resonant interaction between magnetic-field perturbations and betatron oscillations of the beam particles, and takes the form of "snake"-type macroscopic transverse oscillations of the beam which eventually collides with the side wall of the drift chamber. The instability development time is much shorter than the characteristic time for the diffusion of the magnetic field, and the distance over which the instability builds up amounts to a few wavelengths of the betatron oscillations. As the gas pressure increases in the range $1 < P$ (Torr) < 100, the instability development time and length are found to decrease. For beam energy $E = 450$ keV, beam current $I_b \simeq 20$ kA, and beam radius $a \simeq 3$ cm, the instability development time in nitrogen turns out to be 10^{-8}–10^{-9} s, and the corresponding path length is between a few meters and 30 cm. A theoretical model has been developed. It can be used to explain observed phenomena and to calculate the instability parameters which are in good agreement with experimental results.

1. INTRODUCTION

The analysis of instabilities and their propagation in gas or plasma occupies an important place in the theory of transport of high-current beams of relativistic electrons. Experimental studies of the transport of beams with beam current $I_b < I_A$ ($I_A = \gamma\beta m_e c^3/e$ is the Alfven current) in neutral gases, performed at different laboratories, have shown that there is a relatively narrow pressure range in which the beam propagates readily to distances of up to 10 m (Ref. 1). For nitrogen, this pressure range lies near $P \simeq 1$ Torr, where the energy loss is related to the development of beam instability and elastic scattering of the relativistic particles by atoms and ions of the plasma produced by the beam injected into the gas.[2] At moderate pressures $1 < P$ (Torr) < 100, several experiments have shown a loss of beam stability, accompanied by the cutting off of the current and a deterioration in transport properties.[1,3] The observed phenomena are related in Ref. 1 to the development of hose instability.[4]

The hose instability of a beam in finite-conductivity plasma was first examined by Rosenbluth.[5] The instability mechanism is that particles moving in their own magnetic field begin to experience a centrifugal force when the beam is subjected to small random bending perturbations. The displacement of the beam in the lateral direction under the influence of this force, to a characteristic distance of the order of the beam radius, occurs in a time that is greater than the time taken by the magnetic field to diffuse into the ambient plasma: $\tau_d = 4\pi\sigma a^2/c^2$ (σ is the plasma conductivity and a the radius of the beam). This instability model[5] was subsequently developed further in Refs. 4, 6, and 7.

Another type of hose instability was examined by Ivanov and Rudakov.[8] In high-conductivity plasma, the beam and its magnetic field are "frozen" into the ambient plasma. The centrifugal force then displaces the beam in the lateral direction together with the plasma and, as shown in Ref. 8, the rate of propagation of the instability turns out to be of the same order as the velocity of sound. The characteristic features of hose instability are examined in Refs. 5 and 8 where it is shown that the wavelength of this instability is much greater than the wavelength of betatron oscillations of the beam particles.

The "snake" instability with wavelength approaching the betatron wavelength is due to the electrostatic interaction between beam electrons and the ion background, and was considered in Ref. 9 in the "rigid beam" approximation. An instability of a relativistic electron beam that deflects the beam to the wall of the drift chamber was discovered in Ref. 10. The characteristic time for the development of this instability is shorter by more than an order of magnitude than the corresponding time for hose instability, and its wavelength is close to that of the betatron oscillations. The phenomenon was explained in Ref. 10 by the development of resonant resistive instability. Qualitatively, this instability is due to the resonant interaction between betatron oscillations of beam particles in the resultant azimuthal magnetic field $H_{0\varphi}$ produced by the resultant current I_Σ ($I_\Sigma = I_b - I_{\rm pl}$, where $I_{\rm pl}$ is the plasma current) and the magnetic-field perturbations $\delta\mathbf{H}$. When the phase resonance condition $k_z V_z = \omega_{\beta 0}$ is satisfied (k_z is the wave number of the perturbations, V_z is the longitudinal velocity of beam electrons, and $\omega_{\beta 0}$ is the frequency of betatron oscillations), the Lorentz force ensures that the amplitude of the betatron oscillations undergoes a resonant variation with time, which is of the form

$$\xi(t) \sim \frac{\omega_{\beta 0} a}{2} \int \frac{\delta H_\varphi}{H_{0\varphi}}\, dt. \tag{1}$$

When the dependence of the field perturbation on the angle φ is $\delta H \propto e^{i}$ (i.e., we have the mode with azimuthal number $m = 1$), the variation in the amplitudes of the particle oscillations leads to the lateral displacement of the beam as a whole.

This effect is illustrated qualitatively in Fig. 1, which

 0038-5646/84/040747-09$04.00

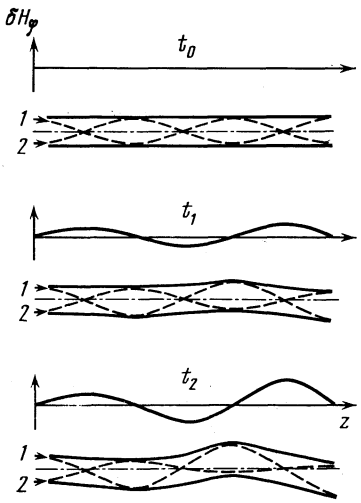

FIG. 1. Change in the trajectories 1, 2 (broken lines) and of the envelope of the particle beam (solid line) under the influence of a perturbation δH_φ of the magnetic field for three successive intervals of time: t_0, t_1, t_2. Dot-dash line shows the axis of the drift chamber.

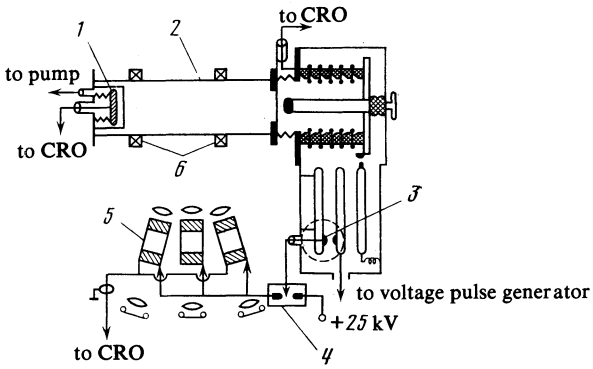

FIG. 2. Schematic diagram of the apparatus: 1—Faraday cup; 2—drift chamber; 3—water-filled discharger; 4—gas-filled discharger; 5—image converter; 6—Rogowski belts.

shows two trajectories (1 and 2) with phase difference of half a period at different instants of time. The paticle moving along trajectory 1 is in phase with the magnetic-field perturbations, and the amplitude of its oscillations is increased by the Lorentz force, whereas the amplitude of the oscillations of particle 2, which are in antiphase, is reduced. The result of this is an asymmetry in the beam-current distribution, which grows in time and in space in the direction of propagation of the beam. If the perturbation in the beam current density is $\delta j_b \sim \xi \partial j_{0b}/\partial r$, the equation for the magnetic field in finite-conductivity plasma is $\frac{\partial \mathbf{H}}{\partial t} = -\operatorname{rot}\left(\frac{c^2}{4\pi\sigma}\operatorname{rot}\mathbf{H} - \frac{c}{\sigma}\mathbf{j}_b\right)$, and (1) yields the following estimate for the instability growth rate for $\tau d/t \gg 1$:

$$t^{-1} \sim \left(\frac{\omega_{p0}}{\tau_d}\frac{I_b}{I_\Sigma}\right)^{1/3} \gg \tau_d^{-1}.$$

In this paper, we present an experimental study of resonant resistive instability of a beam of relativistic electrons, and propose a theoretical model for it.

2. EXPERIMENTAL SETUP AND DIAGNOSTIC EQUIPMENT

The macroscopic instability was investigated experimentally on the "Neptun" accelerator[11] which generated a beam of relativistic electrons with energy $E = 450$ keV. The beam current and pulse length were, respectively, $I_b = 20$ kA and $\tau = 60$ ns. Beam electrons emitted by a flat graphite cathode, 4.8 cm in diameter, were injected through an anode in the form of a 20-μm titanium foil into the drift chamber with an internal diameter of 17 cm. The chamber was filled with nitrogen or helium (Fig. 2). The length of the chamber was varied in these experiments between 3 cm and 3 m, and the pressure range was 1–100 Torr. When the drift chamber was made of plexiglas, the return current lead was a metal wall placed against the inner surface of the chamber. In several experiments, the drift chamber was in the form of a metal tube.

The basic electrical measurements were performed with various designs of the Faraday cup. The radial current density distribution $j_b(r, t)$ in the beam was measured with two modifications of a segmented Faraday cup (SFC). Their design was similar to that described in Ref. 12. In the first of these probes (SFC-1), nine collectors, each of radius 5 mm, were located in a plane perpendicular to the chamber axis and along one of its diameters. The separation between the centers of these collectors was 16 mm. In the second group (SFC–2), ten collectors of the same shape were arranged along three radii at 120° to one another (with three collectors on each radius and one at the center, which was common for all the radii). In all these experiments, the SFC's were mounted at the end of the drift chamber.

Relativistic electrons leaving the beam were recorded by vacuum Faraday cups with collector diameter of 100 mm. They were located on the lateral surface of the drift chamber at different distances from the accelerator exit window, and at different azimuths relative to the chamber axis. To determine the length over which the beam was deflected onto the wall of the drift chamber, we constructed a segmented Faraday cup (SFC-3), consisting of three vacuum probes separated from the gas-filled volume by a thin foil (30 μm thick). These probes were on a plane perpendicular to the chamber axis. The probes were mounted on the surface of the chamber so that their collectors covered almost completely a portion of the lateral surface 8 cm wide. The Faraday cup was designed so that it could be mounted at any distance from the entrance to the chamber. The beam current I_b leaving the drift volume was measured with a vacuum Faraday cup whose collector covered completely the transverse cross section of the chamber. An aluminum foil, 30 μm thick, was used in all the vacuum Faraday cups to separate the evacuated volume of the probes from the drift chamber. The resultant current I_Σ was measured by two integrating Rogowski belts whose design is described in Ref. 13. The signal risetime in the Rogowski belts was 5 ns, and the decay time was 2–3 μs. The belts could be placed at any distance from the point of beam injection.

In addition to the electrical measurements, we also photographed the plasma emission produced in the drift chamber by the beam. This was done with the aid of electro-

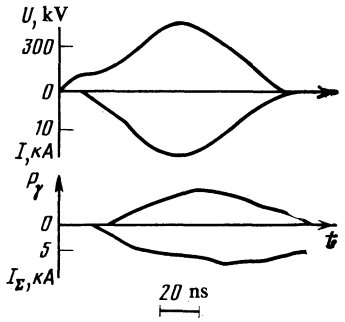

FIG. 3. Oscillograms of the diode voltage U and current I, the signal P from the photomultiplier, and the resultant current I_Σ.

statically-focused imaged converters 5 incorporating fiber-optics plates at entrance and exit. An image reduced by a factor of ten was produced on the converter photocathode by Gelios-40 objectives. The exposure time used for each frame (5 ns) was dictated by the length of the electrical supply pulse (10 kV), which was delivered by a cable oscillator consisting of a single line and a gas discharge 4 (Ref. 14). The discharger was fired by a pulse taken from the shunt in the discharger 3, which acted as a cummutator for the shaping hydraulic line of the accelerator. The time interval between the image converter frames was determined by the difference between the length of the cables delivering the signals from the generator, and amounted to 5 ns. This method enabled us to obtain data on the nature of beam motion. This conclusion was made on the basis of the following experiment. The beam was injected into a 12 cm long Plexiglas tube filled with nitrogen ($P = 30$ Torr). A Faraday cup, a Rogowski belt, and a photoelectron converter with nanosecond resolution were placed in front of the exit window of the accelerator in the immediate neighborhood of one another. The use of short tube enabled us to reduce the inaccuracy in the synchronization of these devices (due to the finite propagation time of the beam in the gas) down to 1 ns. Figure 3 shows oscillograms of the signals produced by these detectors. It is clear that the emission in the visible range appears simultaneously with the beam (to within 1 ns) and vanishes practically simultaneously with the beam current. At the same time, measurements of the resultant current passing through the channel produced by the beam show that this current persists for a much longer time (more than 100 ns). It follows that the beam passing through the gas produces a characteristic "autograph" in the form of optical emission.

In each experiment, we recorded the diode current and voltage, which enabled us to select those events for which the spread in these parameters did not exceed 10%.

3. EXPERIMENTAL DATA

Measurements of the beam charge transport as a function of pressure show that there is a characteristic valley in the transport efficiency, which occurs for pressure $10 < P$ (Torr) < 100. For a given gas, the width and depth of this valley depend on the transport length. An increase in pressure was found to be accompanied by a reduction in the length of the current pulse during the propagation of the beam through the gas. This was also noted in Refs. 1 and 3.

Before the above phenomena could be explained, and a model capable of describing them could be developed we had to perform experiments in which measurements were made of the radial beam density distribution, the loss of relativistic particles to the wall of the drift chamber, and the deterioration in beam transport. The most detailed experiments were performed in nitrogen.

Measurements of the radial distribution of beam current density $j_b(r, t)$ at different distances from the accelerator window at a pressure of $P \sim 1$ Torr showed that the profile of $j_b(r, t)$ remained symmetric relative to the chamber axis for lengths $L \lesssim 0.8$ m (Fig. 4a). Longer transport lengths were accompanied by a departure from the symmetry of the radial profile (see Fig. 4b), and this departure was first noticed on the trailing edge of $j_b(r, t)$. For given pressure, the asymmetry in the beam density distribution was found to increase with increasing transport length and led to the deflection of the beam as a whole from the chamber axis. Thus, whilst, for $P \sim 1$ Torr and distance $L \simeq 2$ m, the deflection of the beam from the axis did not exceed the beam radius, a deflection exceeding the beam radius was recorded at the end of the beam current pulse at a distance of $L \simeq 3$ m.

For fixed lengths $L > 30$ cm, the asymmetry of the current-density profile and the size of the deflection were found to increase with increasing pressure $P > 1$ Torr. Figure 4c shows the time dependence of the radial profile for transport length $L = 85$ cm and $P = 5$ Torr. Whereas at $P = 1$–3 Torr there was only a slight asymmetry in the distribution (see Figs. 4b and c, at $P \geqslant 5$ Torr) the asymmetry increased sub-

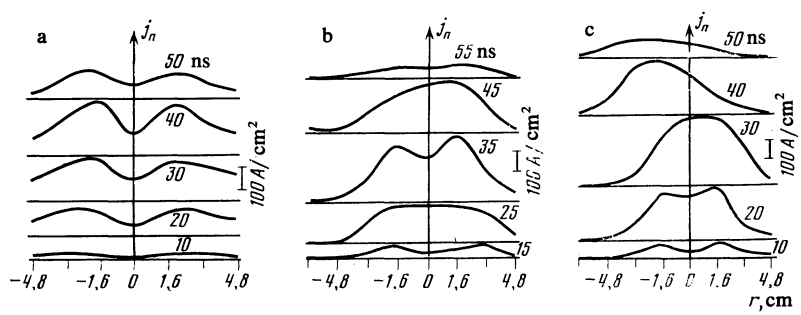

FIG. 4. Radial distribution of beam current density at different times: a—$P = 1$ Torr, $L = 26$ cm; b—$P = 1$ Torr, $L = 85$ cm; c—$P = 5$ Torr, $L = 85$ cm.

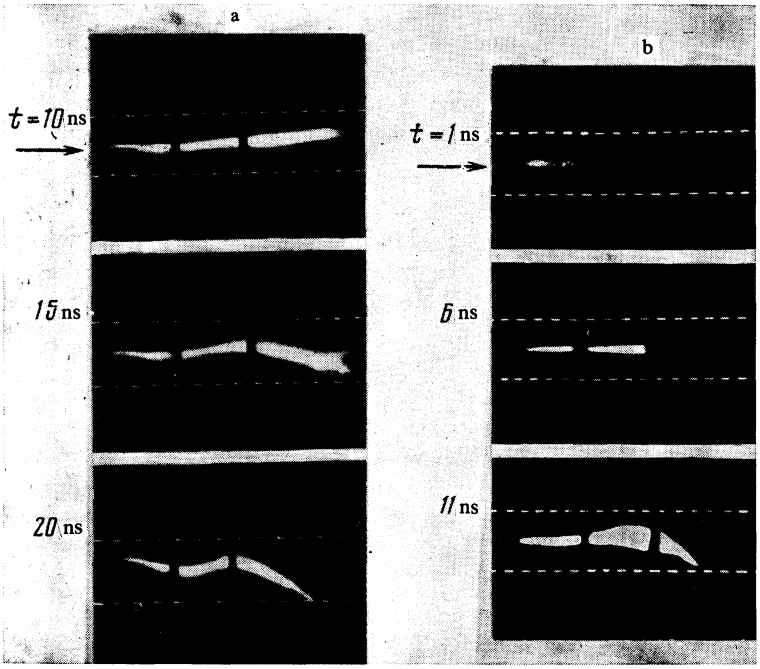

FIG. 5. Photographs taken from the image-converter, showing the deflection of the beam to the wall of the drift chamber: a—$P = 30$ Torr, $L = 1.3$ m; b—$P = 60$ Torr, $L = 1.3$ m; arrow shows the direction of injection of the beam; broken lines correspond to the position of the chamber walls, and the vertical dark bands are distance markers separated by 20 cm (the first marker lies at 40 cm from the anode foil).

stantially and the beam was displaced in the radial direction. The higher the pressure, the earlier the onset of the profile asymmetry and the higher the rate of its growth and of radial deflection.

The data obtained with the aid of the SFCs are in agreement with optical measurements. Figure 5 shows photographs recorded with the image converters as described in Sec. 2. The time was measured from the onset of emission at the center of the tube, which was recorded with the collimated photomultiplier. Measurements showed that this corresponded to the arrival of the beam at the midpoint of the drift tube. It is clear from the photographs that the beam was displaced in the radial direction. The next problem was to determine whether the beam was displaced in a single plane or whether it was helical in shape. This was done by photographing the emission produced by the beam in two mutually perpendicular directions, using two image converters. The experimental arrangement is shown in Fig. 6. Comparison of the two photographs in Fig. 6a shows that the projected beam traces are shifted relative to one another by the distance $\Delta\lambda = 12$ cm, which is equal to a quarter of the wavelength of the beam oscillation ($\lambda = 45$ cm). This confirms the helical shape of the beam. Our experiments thus lead us to the conclusion that the development of instability results in a helical beam trajectory, and that the helix unwinds as the beam approaches the end of the drift chamber.

Analysis of the time dependence of the current-density profile recorded with SFC-2 shows that the resulting asym-

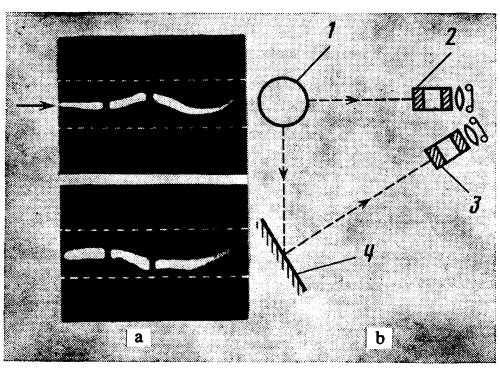

FIG. 6. a—Photographs of the image-converter screen: (arrow shows the direction of the beam injection); b—optical arrangement; 1—camera, 2,3—image converter, 4—mirror.

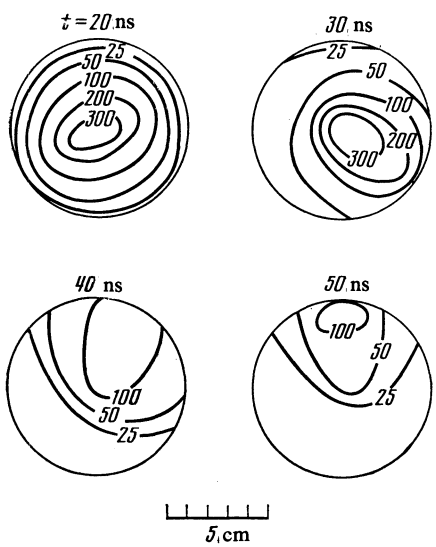

FIG. 7. Beam current density distribution (A/cm^2) at different times.

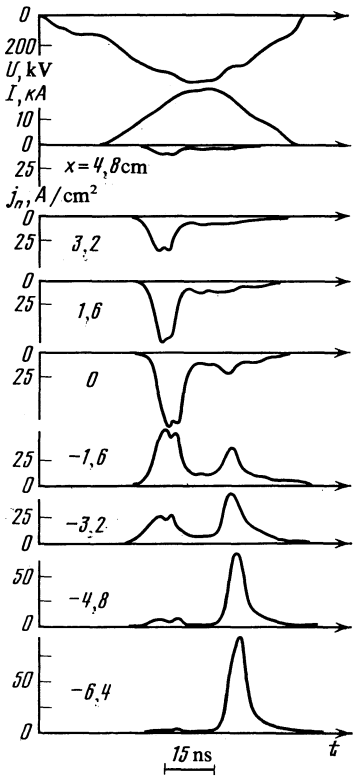

FIG. 8. Oscillograms of the diode voltage U and current I, and the current density j_b from the SFC-1 collectors mounted at different distances x from the chamber axis; $P = 15$ Torr, $L = 85$ cm.

metry is accompanied by the rotation of the beam around its axis. Figure 7 shows the current density distribution in the plane perpendicular to the chamber axis as a function of time. For the sake of clarity, the collector centers intercepting equal electron currents are connected by solid lines. The angular velocity of the beam determined from these measurements was found to be 3×10^8 s^{-1}. Both left- and right-handed beam rotation was observed.

Comparison of the photographs made with the image-converters and integrating photographs also shows that the instability has a weakly convective character, with the drift velocity of the perturbations not exceeding 10^9 cm/s.

For pressures $P > 10$ Torr, the amplitude of transverse oscillations was so large that most of the beam was intercepted by the wall of the drift chamber. Figure 8 shows oscillograms form the collectors of SFC-1, which was mounted at a distance equal to the distance ($L = 85$ cm) at which the beam hit the wall at a pressure of $P = 15$ Torr. The beam deflection dynamics is illustrated in Fig. 8. For the first 15 ns, the beam propagates reasonably symmetrically. After a further 10 ns, it disappears from the field of view of the collectors, then reappears, but only on half the probes. During this process, the beam is deflected in the radial direction with velocity $v_r \sim 10^9$ cm/s. A very similar velocity was obtained in experiments in which the current-density measurements were accompanied by a current of relativistic electrons to the side wall of the chamber.[10]

Measurements performed with SFC-3 show that the distance L over which the beam is deflected to the chamber

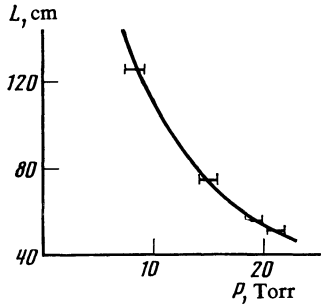

FIG. 9. Distance L for the deflection of the beam to the wall as a function of pressure P.

wall depends on pressure (Fig. 9), and that L decreases with increasing pressure. The fact that, in all these experiments, we always recorded a current of relativistic electrons to only one of the three probes, leads us to the conclusion that the beam as a whole was deflected to the wall.

Photographs made with the image converter confirmed the above results and provided us with additional information on the instability development. Figure 5a shows three successive photographs of the deflection of the beam to the wall of the drift chamber at a pressure $P = 30$ Torr. It is clear from the first frame that, for $10 < t$ (ns) < 15, the beam was near the chamber axis. On the next frame, the beam is displaced in the radial direction to a distance of the order of the radius in a time $15 < t$ (ns) < 20 and, finally, the third frame $[20 < t$ (ns) $< 25]$ shows the interception of the beam by the chamber wall. It follows from Fig. 5a that the characteristic length of the perturbations is $\lambda = 45$ cm. This wavelength decreases with increasing pressure, and, for example, amounts to $\lambda = 30$ cm for $P = 60$ Torr. The characteristic instability development time was found to decrease with increasing pressure. For comparison, Fig. 5b shows the beam deflection dynamics for $P = 60$ Torr. It is clear from the photograph that, in about 1 ns after the appearance of the photomultiplier signal, the beam has traversed a distance of 40 cm from the anode foil. After 6 ns, this distance became 60 cm and the beam was practically undisturbed but, at about 11 ns, it touched the wall. The instability development time in this case did not exceed a few nanoseconds. Analysis of the photographs obtained with the image-converter for different pressures shows that the average transverse displacement velocity increases with increasing pressure. As the pressure was varied from 5 to 60 Torr, the velocity was found to rise from 5×10^8 to 2×10^9 cm/s.

We have found that there is a critical distance from the point of injection (approximately 30 cm) over which the beam remains undisturbed. This is in agreement with electrical measurements in which it was established that, for lengths shorter than the critical value, the deflection of the beam to the chamber wall was not observed. This length is equal to the wavelength of betatron oscillations of the electron beam.

The magnetic-field diffusion time in the pressure range employed in our experiments ($a = 3$ cm, $\sigma \gtrsim 10^{12}$ s^{-1}) exceeds 100 ns (Ref. 15). Hence, it follows from the experimental results that the instability that we have investigated de-

velops in a time that is much shorter than the magnetic-field diffusion time, i.e., $t \ll \tau_d$. Since the magnetic field is "frozen" into the plasma channel produced by the beam, the resultant current I_Σ flowing through the channel does not vary along the chamber as the beam is deflected to the wall. This is in agreement with measurements of the resultant current made with the two Rogowski belts positioned as shown in Fig. 2. The distance between the point of injection and the first and second belts was 30 cm and 70 cm, respectively. A vacuum Faraday cup was placed at a distance of 7 cm from the second Rogowski belt. The pressure was chosen so that the beam was deflected to the wall between the two Rogowski belts. It follows from the experimental results that, when the beam is deflected to the wall, the resultant current does not vary with distance from the accelerator exit window. When the beam is injected into helium, the instability develops at higher pressures ($P \gtrsim 25$ Torr) as compared with nitrogen. It follows from the experimental results that, in the pressure range that we have investigated, the amplitude of transverse beam displacements did not exceed the radius of the chamber and there was practically no deflection of the beam to the wall.

4. THEORY OF RESONANT RESISTIVE INSTABILITY OF A RELATIVISTIC ELECTRON BEAM IN PLASMA

We shall consider the stability of a relativistic electron beam within the framework of the Vlasov transport equation with self-consistent fields but without the collision integral, which is valid for sufficiently tenuous plasma. If the characteristic time of instability development is such that $\sigma t \ll 1$, and the beam particle density is much less than the plasma density, $n_b \ll n_{pl}$, the effect of electrostatic fields on the motion of beam particles and the displacement currents in Maxwell's equations can be neglected. The basic set of equations can then be written in the form

$$\frac{\partial f}{\partial t}+\frac{\mathbf{p}}{\gamma m_e}\nabla f+\frac{e}{c}\left(-\frac{\partial \mathbf{A}}{\partial t}+\frac{1}{\gamma m_e}\mathbf{p}\times\mathrm{rot}\,\mathbf{A}\right)\frac{\partial f}{\partial \mathbf{p}}=0,$$

$$\frac{\sigma}{c}\frac{\partial \mathbf{A}}{\partial t}-\frac{c}{4\pi}\Delta\mathbf{A}=\mathbf{j}_b,\quad \mathbf{j}_b=e\int\frac{\mathbf{p}}{\gamma m_e}f d^3\mathbf{p},\quad \mathrm{div}\,\mathbf{A}=0,$$

where f is the beam particle distribution function and $\mathbf{A}$ is the vector potential of the electromagnetic field.

Linearizing the basic set of equations relative to the equilibrium values f_0 and A_0 for $\omega a/c \ll k_z a \ll 1$, $p_\perp \ll p_z$, we obtain the following set of equations for the perturbation δf of the distribution function and the perturbation δA_z of the z component of the vector potential:

$$\frac{\partial \delta f}{\partial t}+\frac{\mathbf{p}}{\gamma m_e}\nabla\delta f+\frac{e}{\gamma m_e c}\times\left\{\mathbf{p}\times\mathrm{rot}\,\mathbf{A}_0\frac{\partial \delta f}{\partial \mathbf{p}}+\nabla_\perp(p_z\delta A_z)\frac{\partial f_0}{\partial \mathbf{p}_\perp}\right\}=0, \tag{2}$$

$$\frac{\sigma}{c}\frac{\partial \delta A_z}{\partial t}-\frac{c}{4\pi}\Delta\delta A_z=\delta j_z, \tag{3}$$

$$\delta j_z=e\int\frac{p_z}{\gamma m_e}\delta f d^3\mathbf{p}. \tag{4}$$

Integrating (2) along the trajectories of undisturbed motion, and substituting δf in (4), we obtain

$$\delta j_z=-e^2\int\frac{p_z}{\gamma^2 m_e^2 c}\int_{-\infty}p_z\frac{\partial \delta A_z}{\partial \mathbf{r}_\perp}\frac{\partial f_0}{\partial \mathbf{p}_\perp}dt d^3\mathbf{p}. \tag{5}$$

To evaluate the integral in (5), we must know the equations of the undisturbed trajectories and the equilibrium distribution function for the beam particles.

We shall consider a cylindrical beam of radius a, propagating in the direction of the z axis in plasma that occupies uniformly the space (r, φ, z). In the original (undisturbed) state, the beam particles travel along the z axis, executing transverse (betatron) oscillations of frequency ω_β. Since we are assuming that $\omega_\beta \tau_d \gg 1$, we may suppose that the motion of beam electrons takes place in the quasistatic magnetic field $H_\varphi(r) = \mathrm{rot}_\varphi A_0$ due to the beam and the plasma currents, so that the particle energy is conserved: $\gamma m_e c^2 = \mathrm{const}$. Moreover, since the magnetic field is axially and azimuthally uniform, the z components of the generalized and angular momenta are conserved:

$$\mathscr{P}_z=p_z+\frac{e}{c}A_{0z}=\mathrm{const}\equiv\gamma\beta m_e c-\frac{\varepsilon}{\gamma\beta c},\quad \beta=\left(\frac{\gamma^2-1}{\gamma^2}\right)^{1/2}, \tag{6}$$

$$M_z=p_\varphi r=\mathrm{const}\equiv M.$$

The ratio ε/γ has the significance of the energy of lateral motion. For times $t < \tau_d$, the distribution of the magnetic field is determined both by the distribution of the beam current and of the induced current of plasma electrons. We shall take the vector potential within the beam ($r \leqslant a$) in the form

$$A_{0z}=-\frac{I_\Sigma}{I_A}\frac{\gamma\beta m_e c^2}{ea^2}r^2. \tag{7}$$

Particle oscillations described by (6) in the field (7) are nonlinear, and the associated trajectories must be expressed in terms of the Jacobi elliptic functions. We shall examine the case where $p_z \gg p_\perp$,

$$\frac{\varepsilon}{\gamma^2\beta^2 m_e c^2}\sim\frac{I_\Sigma}{I_A}\ll 1,$$

$$M\ll\frac{\varepsilon a}{\gamma\beta c}\left(\frac{I_A}{I_\Sigma}\right)^{1/2},$$

where the particle coordinates $[r(t), \varphi(t), z(t)]$ can be approximately written in the form

$$r^2=a^2\left\{\frac{M^2}{2\varepsilon m_e a^2}+\left(\frac{\varepsilon}{\varepsilon_{max}}-\frac{M^2}{m_e\varepsilon a^2}\right)\cos^2\omega_\beta(t+t_0)\right\}, \tag{8}$$

$$\varphi-\varphi_0=\mathrm{arctg}\left\{\left[\frac{M^2\varepsilon_{max}}{2\varepsilon^2 m_e a^2}\left(1-\frac{\varepsilon_{max}M^2}{2\varepsilon^2 m_e a^2}\right)^{-1}\right]^{1/2}\mathrm{tg}\,\omega_\beta(t+t_0)\right\}, \tag{9}$$

$$z-z_0=c\beta t\left(1-\varepsilon/2\gamma^2\beta^2 m_e c^2\right), \tag{10}$$

t_0, φ_0, z_0 are integration constants, $\varepsilon_{max} = -e\gamma\beta A_{0z}(a)$, and

$$\omega_\beta=\omega_{\beta 0}\left(1-\frac{\varepsilon}{8\gamma^2\beta^2 m_e c^2}\right),$$

$$\omega_{\beta 0}=\frac{c\beta}{a}\left(\frac{2I_\Sigma}{I_A}\right)^{1/2}.$$

Equations (8)–(10) describe the trajectory of a beam particle

in the form of an elliptical helix, whose pitch depends on the amplitude.

The equilibrium distribution function f_0, which depends on the constants of motion, will be taken in the form

$$f_0=\delta(\gamma-\gamma_0)\,\Phi\left(\frac{\gamma_0\beta_0 m_e c-\mathscr{P}_z}{\bar{\varepsilon}}\gamma_0\beta_0 c\right)\Psi\left(\frac{M_z}{\bar{M}}\right), \qquad (11)$$

where Φ and Ψ are arbitrary functions, and the parameters $\bar{\varepsilon}$ and $\bar{M}$ characterize the spread of the generalized and angular momenta of beam particles:

$$\bar{M}\ll\frac{a\bar{\varepsilon}}{\gamma\beta c}\left(\frac{I_A}{I_\Sigma}\right)^{1/2}.$$

We must now determine the perturbation of the beam current density (5). We shall suppose that the perturbations δj_z and δA_z are functions of coordinates and time, as follows:

$$\{\delta j_z,\ \delta A_z\}=\{\delta j_z(r,\varphi),\ \delta A_z(r,\varphi)\}\exp(-i\omega t+ik_z z).$$

We shall confine our attention to fast processes for which $\omega\tau_d\gg 1$. The perturbation of the vector potential outside the beam is then negligible, and the condition on the boundary of the beam is $\delta A_z\,(r,\varphi)|_{r=a}=0$. In the interior of the beam, and right up to the boundary ($r\ll a$), we have the expansion

$$\delta A_z(r,\varphi)=e^{im\varphi}\sum_{k=1}^{\infty}A_k J_m\left(\mu_k\frac{r}{a}\right), \qquad (12)$$

where μ_k is the k th positive root of the Bessel function of order m. The current density perturbation will also be taken in the form of an expansion:

$$\delta j_z(r,\varphi)=e^{im\varphi}\sum_{\varkappa=1}^{\infty}j_\varkappa J_m\left(\mu_\varkappa\frac{r}{a}\right),$$

where the expansion coefficients are given by

$$j_\varkappa=\frac{2}{a^2J_{m+1}^2(\mu_\varkappa)}\int_0^a\delta j_z(r,\varphi)\,e^{-im\varphi}J_m\left(\mu_\varkappa\frac{r}{a}\right)r\,dr. \qquad (13)$$

We now substitute the current density perturbation (5) and use (11) and (12), so that, after integrating along the trajectories (8)–(10) with respect to the momenta and coordinates, we finally obtain

$$j_\varkappa=-\frac{4\pi\beta m_e c^2e^2}{a^2}\sum_{k=1}^{\infty}\sum_{n=-\infty}^{\infty}\frac{nA_k\cos^2[1/2(m+n)\pi]}{J_{m+1}^2(\mu_\varkappa)}$$

$$\times\int_0^1\frac{dv}{n\omega_\beta(v)+k_zV_z(v)-\omega}$$

$$\times\left\{\frac{1}{2}\frac{\partial}{\partial v}\Phi\left(v^2\frac{\varepsilon_{max}}{\bar{\varepsilon}}\right)S_{\varkappa k}-\frac{m}{4n}\Phi\left(v^2\frac{\varepsilon_{max}}{\bar{\varepsilon}}\right)T_{\varkappa k}\right\}, \qquad (14)$$

$$S_{\varkappa k}=U_\varkappa(v)\,U_k(v),\qquad T_{\varkappa k}=U_\varkappa(v)\,W_k(v)+U_k(v)\,W_\varkappa(v),$$

where we have introduced the dimensionless variable $v=(\varepsilon/\varepsilon_{\max})^{1/2}$ and

$$\omega_\beta(v)=\omega_{\beta0}\left(1-v^2\frac{\varepsilon_{max}}{8\gamma^2\beta^2m_ec^2}\right),$$

$$V_z(v)=c\beta\left(1-\frac{v^2\varepsilon_{max}}{2\gamma^2\beta^2m_ec^2}\right)$$

are, respectively, the frequency of betatron oscillations and the average velocity along the z direction of particles with lateral energies $\varepsilon=v^2\varepsilon_{\max}$. We have also introduced the dimensionless function

$$U_k(v)=J_{\frac{m-n}{2}}\left(\frac{\mu_k v}{2}\right)J_{\frac{m+n}{2}}\left(\frac{\mu_k v}{2}\right),$$

$$W_k(v)=J_{\frac{m-n}{2}}\left(\frac{\mu_k v}{2}\right)\frac{\partial}{\partial v}J_{\frac{m+n}{2}}\left(\frac{\mu_k v}{2}\right)-J_{\frac{m+n}{2}}\left(\frac{\mu_k v}{2}\right)\frac{\partial}{\partial v}J_{\frac{m-n}{2}}\left(\frac{\mu_k v}{2}\right). \qquad (15)$$

In the expression for $j_\varkappa$, the term containing the derivative of the distribution function is connected with the change in the energy of transverse motion, whereas the term proportional to the distribution function is connected with the change in the angular momentum of the beam particles about the z axis, which occurs only for perturbations that are inhomogeneous in the angle φ (i.e., for $m\neq 0$).

Let us consider (3), into which, after the transformation given by (12), we substitute $j_\varkappa$ (14):

$$\left\{-i\omega\sigma+\frac{c^2}{4\pi}\left(\frac{\mu_\varkappa^2}{a^2}+k_z^2\right)\right\}A_\varkappa$$

$$=-\frac{4\pi\beta m_ec^3e^2}{a^2J_{m+1}^2(\mu_\varkappa)}\sum_{k=1}^{\infty}\sum_{n=-\infty}^{\infty}nA_k\cos^2\left(\frac{m+n}{2}\pi\right)$$

$$\times\int_0^1\left(\frac{1}{2}\frac{\partial\Phi}{\partial v}S_{\varkappa k}-\frac{m}{4n}\Phi T_{\varkappa k}\right)[n\omega_\beta(v)+k_zV_z(v)-\omega]^{-1}\,dv. \qquad (16)$$

The presence of the factor $\cos^2[1/2(m+n)\pi]$ in (16) shows that the current-density perturbation in the beam is nonzero only for modes with the same m and n parity.

The right-hand side of (16) contains the denominator $(\omega-k_zV_z-n\omega_\beta)$ and, when the phase resonance condition $\omega-k_zV_z=n\omega_\beta$ is satisfied, the beam particles undergo a resonant interaction with periodic perturbations of the magnetic field, and excitation of the instability may be expected.

We shall examine (16) in two limiting cases.

(1) Let us suppose that the spread $\bar{\varepsilon}$ is small, i.e.,

$$|\omega-k_zV_z-n\omega_\beta|\gg\frac{\bar{\varepsilon}}{\gamma^2\beta^2m_ec^2}\left|\frac{4k_zc\beta+n\omega_{\beta0}}{8}\right|. \qquad (17)$$

Suppose that, for a certain $n=n_{\rm res}$, both (17) and the following resonance condition are satisfied:

$$\left|\frac{\omega-k_zc\beta-n\omega_{\beta0}}{\omega_{\beta0}}\right|\ll 1. \qquad (18)$$

It is then sufficient to retain only the term with $n=n_{\rm res}$ in the sum over n in (16) and, since the spread $\bar{\varepsilon}$ is unimportant, the resonance denominator can be taken outside the integral sign.

To explain the experimental results on macroscopic instability, we shall confine ourselves to the case where m and $|n|$ are small, and consider fast processes for which $|\omega\tau_d|\gg m^2n^2$. Small-scale perturbations with $\mu_k>|\omega\tau_d|^{1/2}$ on the right-hand side of (16) can be neglected because they are dissipated by diffusion during the instability develop-

ment time ω^{-1}. Equation (16) then yields the following dispersion relation:

$$i\omega\tau_d(\omega-k_z c\beta-n\omega_\beta)=4\pi(I_b/I_\Sigma)\,\omega_{\beta 0}\lambda, \tag{19}$$

where λ is an eigenvalue of the matrix $\{a_{\varkappa k}\}$ with dimensionless elements

$$a_{\varkappa k}=\frac{m_e e I_\Sigma}{\omega_{\beta 0}}\cos^2\left(\frac{m+n}{2}\pi\right)\left[J_{m+1}^2(\mu_\varkappa)\int f_0 d^3\mathbf{p}\,r\,dr\right]^{-1}$$

$$\times\int_0^1\Phi\left\{\frac{\partial}{\partial v}S_{\varkappa k}n+\frac{m}{2}T_{\varkappa k}\right\}dv.$$

It follows from (19) that the instability growth rate has a maximum for $k_z=-n\omega_{\beta 0}/c\beta$ and is given by

$$\mathrm{Im}\,\omega=\left(\frac{4\pi I_b}{I_\Sigma}\frac{\omega_{\beta 0}}{\tau_d}\right)^{1/3}\mathrm{Im}(-i\lambda)^{1/3}. \tag{20}$$

By virtue of (17), all the beam particles are then in resonance conditions with the field oscillations. Expression (20) is identical to within a numerical factor with the estimated growth rate obtained on the basis of qualitative considerations for the mode with $m=|n|=1$. The growth rate that we have obtained exceeds the reciprocal of the diffusion time by the factor $[(I_b/I_\Sigma\omega_{\beta 0}\tau_d]^{1/2}\gg 1$.

When the resonance condition (18) is not satisfied, the growth rate is comparable with τ_d^{-1}.

2. When the condition opposite to that given by (17) is satisfied for certain $n=n_{\mathrm{res}}$ and $v=v_{\mathrm{res}}$, namely

$$|\omega-k_z V_z(v)-n\omega_\beta(v)|\ll\frac{\bar\varepsilon}{\gamma^2\beta^2 m_e c^2}\left|\frac{4k_z c\beta+n\omega_{\beta 0}}{8}\right|, \tag{21}$$

i.e., only particles with energy ε lying in the neighborhood $\delta\varepsilon\sim\gamma^2\beta^2 m_e c^2|\omega|/\omega_{\beta 0}\ll\bar\varepsilon$ of the point $\varepsilon_{\mathrm{res}}=v^2_{\mathrm{res}}\varepsilon_{\max}$ are in resonance with the field. By virtue of (18), it is then sufficient to retain the term with $n=n_{\mathrm{res}}$ in the sum over n in Eq. (16). This term exceeds all the other terms in the sum by the factor $\gamma^2\beta^2 m_e c^2/\bar\varepsilon\gg 1$. For reasons indicated above, we retain a finite number of terms in the sum over k ($\mu_k<|\omega\tau_d|^{1/2}$).

Comparing the right- and left-hand sides of (16) for $k_z V_z\approx -n\omega_\beta\gg\omega$ and $\omega\tau_d\gg 1$, we can write

$$-i\omega\tau_d=(4\pi I_b I_A/I_\Sigma^2)\lambda(k_z), \tag{22}$$

where $\lambda(k_z)$ is an eigenvalue of $\{v_{\varkappa k}\}$ for given k_z and

$$b_{\varkappa k}=-m_e e I_\Sigma^2\cos^2\left(\frac{m+n}{2}\pi\right)\left[I_A J_{m+1}^2(\mu_\varkappa)\int f_0 d^3\mathbf{p}\,r\,dr\right]^{-1}$$

$$\times\int_0^1\left(n\frac{\partial\Phi}{\partial v}S_{\varkappa k}-\frac{m}{2}\Phi T_{\varkappa k}\right)[n\omega_\beta(v)+k_z V_z(v)]^{-1}\,dv. \tag{23}$$

The instability occurs for $\mathrm{Re}\,\lambda>0$. It is clear form (23) that, whatever the sign of the derivative $\partial\Phi//\partial v$, we can find k_z in the range

$$0\leqslant|n|\frac{\omega_{\beta 0}}{c\beta}-|k_z|\leqslant\frac{3}{8}\frac{\varepsilon_{max}}{\gamma^2\beta^2 m_e c^2}\frac{\omega_{\beta 0}}{c\beta}|n|$$

such that the signs of the principal parts of the integrals of the diagonal elements of the matrix (23) will be positive, so that we shall have λ with a positive real part.

For the "snake" mode ($m=1$) with wavelength approaching the betatron wavelength ($n=1$), the growth rate is particularly high, and this occurs for wavenumber $k_z=\pm\omega_{\beta_0}/c\beta$, i.e., for $v_{\mathrm{res}}\to 0$ in (21). The numerator in the integrand in (16) for $v\to 0$ is then proportional to $v^{|m-n|+|m+n|-1}=v$, and the integral increases logarithmically with increasing

$$3\bar\varepsilon\omega_{\beta 0}/8\gamma^2\beta^2 m_e c^2|\omega-k_z c\beta\pm\omega_{\beta 0}|.$$

Neglecting the spread in the frequency of oscillation of electrons with different angular momenta:

$$\mathrm{Im}\,\omega\gg\bar M/a^2\gamma m_e,$$

and assuming that

$$|\omega\tau_d|>\frac{3}{8}\frac{\bar\varepsilon}{\gamma^2\beta^2 m_e c^2}\frac{\omega_{\beta 0}}{|\omega|}\gg 1$$

we obtain the dispersion relation

$$\omega\tau_d=\frac{4}{3}i\frac{I_b I_A}{I_\Sigma^2}g\ln(iR)\Sigma, \tag{24}$$

where

$$R=3/8 n\bar\varepsilon\omega_{\beta 0}/\gamma^2\beta^2 m_e c^2(n\omega_{\beta 0}+k_z c\beta-\omega)\gg 1,\quad n=\pm 1$$

$$g=\varepsilon_{max}\Phi|_{v=0}/\bar\varepsilon\langle\Phi\rangle,\quad\langle\Phi\rangle=\int_0^{\varepsilon_{max}/\bar\varepsilon}\Phi(x)\,dx,$$

$$\Sigma=\sum_{k=1}^{k}\frac{\mu_k^2}{J_2^2(\mu_k)},\qquad\mu_k\sim|R|^{1/3}.$$

In our experiments, the beam is injected into the plasma at one end of the drift chamber. This means that both the development of perturbations in time and amplification of oscillations in space can take place.

To determine the space-time picture of the development of the resonance instability for the dispersion relations (19) and (24), we substitute $\omega\to i\partial/\partial t$, $k_z\to -i\partial/\partial z$ and apply the resulting operators to the beam current-density perturbation $\delta j_z(z,t)$, which we assume to be close to the resonance value i.e.,

$$\delta j_z(z,t)=j(z,t)\exp\left(-i\frac{\omega_{\beta 0}}{c\beta}z\right),$$

where $j(z,t)$ is a slowly-varying function of z. For $j(z\,t)$ we then obtain the following two equations ($m=n=1$):

$$\left(\frac{\partial}{\partial t}+c\beta\frac{\partial}{\partial z}\right)\frac{\partial}{\partial t}j=2i\alpha\frac{\omega_{\beta 0}}{\tau_d}j,\qquad\alpha=\frac{2\pi I_b}{I_\Sigma}\lambda, \tag{25}$$

$$\frac{\partial}{\partial t}j=-\frac{\eta I_A}{I_\Sigma\tau_d}\left\{\ln\frac{\partial/\partial t+c\beta\partial/\partial z}{\zeta\omega_{\beta 0}}\right\}j,$$

$$\eta=\frac{4}{3}\frac{I_b}{I_\Sigma}g\Sigma,\qquad\zeta=\frac{3}{8}\frac{I_\Sigma}{I_A}. \tag{26}$$

The self-similar solutions of (25) and (16) can be written (to within a constant factor) as follows:

$$j(z,t)=J_0\left\{\left(\frac{8i\alpha\omega_{\beta 0}z(t-z/\beta c)}{c\beta\tau_d}\right)^{1/2}\right\}, \tag{25'}$$

$$j(z,t)=\exp\left[\frac{I_A}{I_\Sigma}\frac{\eta}{\tau_d}\left(t-\frac{z}{\beta c}\right)\ln\frac{z\omega_{\beta 0}\zeta}{c\beta}\right]$$

$$\times\left\{\Gamma\left[1+\frac{I_A}{I_\Sigma}\frac{\eta}{\tau_d}\left(t-\frac{z}{\beta c}\right)\right]\right\}^{-1}, \tag{26'}$$

where $\Gamma(x)$ is the gamma function.

5. DISCUSSION

Our experimental and theoretical study of the propagation of a high-current relativistic beam in plasma produced by the injection of a beam into a gas at pressures $P > 1$ Torr has shown that a fast macroscopic beam instability leading to an abrupt deterioration in beam transport will occur. The result of the instability is that the beam as a whole is spontaneously deflected in the transverse direction. In our view, this instability is due to the resonant interaction between beam particles executing betatron oscillations and periodic perturbations of the magnetic field in finite-conductivity plasma (the resonance condition is $k_z \approx \omega_{\beta 0}/c\beta$).

The instability develops much more rapidly than magnetic-field diffusion because of the finite conductivity of the plasma. Hence, the deflection of the beam to the wall of the drift chamber in the time $\Delta t \ll \tau_d$ is accompanied by only a slight change in the current flowing through the chamber:

$$\Delta I_\Sigma < \frac{\Delta t}{\tau_d} I_b \ll I_\Sigma,$$

This has been verified by measurements of I_Σ before and after the deflection of the beam to the wall.

The instability development time and length vary with the conductivity of the ionized gas, and hence, depend on the pressure and type of gas. In nitrogen at pressures in the range $1 < P$ (Torr) < 10, appreciable deflection of the beam from the axis of the drift chamber occurs over a distance of about 1 m in a time comparable with the length of the pulse. The associated conductivity is then $\sigma \sim 10^{13}\,\mathrm{s}^{-1}$ (Ref. 15), and the development of the mode with azimuthal number $m = 1$ and wavelength equal to the betatron wavelength ($n = 1$) proceeds during the linear stage in accordance with (26′):

$$\delta j_z(z,t) \sim \exp\left(-i\frac{\omega_{\beta 0}}{\beta c}z\right)\exp\left[\frac{I_A}{I_\Sigma}\frac{\eta}{\tau_d}\left(t-\frac{z}{c\beta}\right)\ln\frac{3z\omega_{\beta 0}I_\Sigma}{8c\beta I_A}\right] \times\left\{\Gamma\left[1+\frac{I_A}{I_\Sigma}\frac{\eta}{\tau_d}\left(t-\frac{z}{\beta c}\right)\right]\right\}^{-1}. \quad (27)$$

For comparison, let us take the trial distribution function for the beam particles to be the monoenergetic function with the Bennett profile. For $I_\Sigma/I_b \approx 0.4$, $I_b/I_A \approx 0.6$, and $\beta \simeq 0.8$, we then obtain $\eta \sim 100$. The time for the development of the instability over a distance of a few betatron wavelengths is then $\sim 10^{-8}$ s.

An increase in the pressure $P > 10$ Torr and, correspondingly, a reduction in the conductivity ($\sigma \sim 10^{12}\,\mathrm{s}^{-1}$) is accompanied by a change in the development of the current-density perturbations, which now assumes the form (25′):

$$\delta j_z(z,t) \sim \exp\left(-i\frac{\omega_{\beta 0}}{\beta c}z\right) J_0\left\{\left[\frac{8i\alpha\omega_{\beta 0}}{\beta c\tau_d}z\left(t-\frac{z}{c\beta}\right)\right]^{1/2}\right\} \quad (28)$$

where, for the chosen trial distribution function and $I_\Sigma/I_b \approx 0.6$, $I_b/I_A \approx 0.6$ we have $a \simeq 40$. Estimates of the instability development time give about 10^{-9}s even for a distance of the order of the betatron wavelength. Experimentally, the instability is found to develop in a time $\sim 10^{-9}$ s, and the beam is deflected to the wall of the drift chamber over a distance of the order of the betatron wavelength (~ 30 cm).

As a result of the instability, the beam propagates along an unwinding helix whose pitch corresponds to the wavelength of the betatron oscillations of the particles. The observed rotation of the trace of the beam in the plane of the section through the drift chamber with angular velocity $\omega \simeq 3 \times 10^8$ s is in qualitative agreement with (28), where the real part of the frequency is of the same order as the imaginary part.

In the gas-pressure range that we have investigated, the instability in helium develops more slowly and occurs without the beam being deflected to the wall. Actually, the estimated balance of plasma electrons shows that the dependence of σ on the type of gas for pressure $P > 1$ Torr is described by $\sigma \sim B^{-1}$, where B is the coefficient in the Townsend formula.[16] In helium ($B_{He} \simeq 25$), the conductivity is therefore greater by an order of magnitude than in nitrogen ($B_{N_2} \simeq 250$).[17] Since the characteristic instability-development time is approximately proportional to σ (27), it is greater in helium by an order of magnitude as compared with nitrogen, and turns out to be comparable with the length of the beam current pulse in the pressure range that we have investigated.

The authors are grateful to L. I. Rudakov for fruitful discussions.

[1]P. J. Briggs, J. C. Clark, I. J. Fessinden, *et al.*, Proc. Second Intern. Topical Conf. on High Power Electron and Ion Beam, Ithaca, New York Cornell University, 1977, Vol. 2, p. 319.
[2]Yu. V. Tkach, I. I. Magda, G. V. Skachek, *et al.*, Fiz. Plazmy **5**, 586 (1980) [Sov. J. Plasma Phys. **5**, 321 (1980).
[3]G. I. Kotlyarevskiĭ, A. I. Ryabchikov, and Yu. P. Usov., Fiz. Plazmy **2**, 689 (1976) [Sov. J. Plasma Phys. **2**, 380 (1976)].
[4]E. P. Lee, Phys. Fluids **21**, 1327 (1978).
[5]M. N. Rosenbluth, Phys. Fluids **3**, 932 (1960).
[6]S. Weinberg, J. Math. Phys. (Cambridge, Mass.) **8**, 614 (1967).
[7]H. S. Uhm and M. Lampe, Phys. Fluids **23**, 1574 (1980).
[8]A. A. Ivanov and L. I. Rudakov, Zh. Eksp. Teor. Fiz. **58**, 1332 (1970) [Sov. Phys. JETP **31**, 715 (1970)].
[9]B. V. Chirikov, J. Nucl. Energy C **8**, 455 (1966).
[10]L. E. Aranchuk, V. D. Vikharev, V. V. Gorev, *et al.*, Pis'ma Zh. Eksp. Teor. Fiz. **36**, 331 (1982) [JETP Lett. **36**, 405 (1982)].
[11]S. S. Kingsen, G. P. Maksimov, Yu. L. Sidorov *et al.*, Prib. Tekh. Eksp. No. 3, 26 (1973).
[12]R. L. Schuch and I. Y. Kelly, Rev. Sci. Instrum. **43**, 1097 (1972).
[13]D. G. Pellinen, M. S. DiCapua, S. E. Sampayan, *et al.*, Rev. Sci. Instrum. **51**, 1535 (1980).
[14]L. E. Aranchuk, L. A. Dorokhin, E. V. Znatnov, *et al.*, Prib. Tekh. Eksp. No. 5, 138 (1982).
[15]K. V. Kosmachevskiĭ, Raznostnye metody matematicheskoĭ fiziki (Difference Methods in Mathematical Physics), Moscow State University, 1981, p. 91.
[16]V. L. Granovskiĭ, Elektricheskiĭ tok v gaze (Electrical Current in Gases. The Steady-State Current), Nauka, Moscow, 1971, p. 74.
[17]S. S. Kingsen, I. V. Novobrantsev, L. I. Rudakov, *et al.*, Zh. Eksp. Teor. Fiz. **63**, 2132 (1972) [Sov. Phys. JETP **36**, 1125 (1973)].

Translated by S. Chomet